Appendix A

The iLand wildfire module

Development goals

The main goal in developing a wildfire module for iLand, the individual-based forest landscape and disturbance model (Seidl et al. 2012a, 2012b), was to simulate forest fire regimes as an emergent property of topography, climate, and vegetation. In order to enable the investigation of climate change effects on the fire regime a process-based framework was chosen (see Seidl et al. 2011), modeling the principal processes of ignition, spread, vegetation impact, and extinction explicitly. Furthermore, the module should be able to simulate the complex and heterogeneous fire patterns characteristic for mixed severity fire regimes (Perry et al. 2011) as an emergent property of the system, making use of the high spatial resolution of iLand and the ability to account for processes of fire susceptibility down to the level of individual trees. However, considering the general purpose of the iLand simulation platform as tool for scenario analysis with regard to forest landscape dynamics (Seidl et al. 2012a, 2012b), a detailed simulation of e.g., fire behavior (such as described by Andrews et al. 2005) was outside the scope of our modeling. Considering the large amount of experience with wildfire modeling in forest landscape simulators (Keane et al. 2004, Seidl et al. 2011) we did not venture to develop a novel wildfire simulation approach but rather based our modeling on previous works (in particular that of Wimberly (2002), Schumacher et al. (2006), Wimberly and Kennedy (2008), and Keane et al. (2011)), as adapted to the structure of iLand and the context of the development goals described above.

Fire ignition

Fire ignition modeling in iLand is based on the approach of FireBGC v2 (Keane et al. 2011). Fuel availability, fire weather, fire suppression, and historical fire probability influence fire ignition. A minimum threshold of 0.05 kg fuel biomass per meter squared is required in order for a fire to ignite (see the description of fuel modeling below). The base fire ignition probability (P_{base}) is derived as the inverse of the site-specific fire return interval (i.e., the number of years between fires for all land area within a site; Keane et al. 2011), modified to account for landscape area and fire size (Eq. A1).

$$P_{base} = \frac{1}{MFRI_i} \cdot r_{fire} \qquad \text{Eq. A1}$$

with

$$r_{fire} = \frac{cell}{size_i}$$

and $MFRI_i$ the mean fire return interval at cell i, $size_i$ the average fire size, and *cell* the pixel size of the fire simulations (here: 20m × 20m). Fire weather and fire management modify the base fire probability (see Wimberly and Kennedy 2008). Fire weather is characterized by the Keetch Byram Drought Index (*KBDI*) (Keetch and Byram 1968, Keane et al. 2011). The *KBDI* calculates a simplified water balance for the fuel layer and ranges from 0 (no drought) to 800 (severe drought). *KBDI* is updated daily by subtracting the rainfall reaching the forest floor (i.e., after interception losses have been accounted for), and by adding a drying factor computed from maximum daily temperature and mean annual precipitation. To modify the ignition probability in accordance with the fire weather of every simulation year we calculate an annual fire weather index as cumulative sum over the daily *KBDI* values, and relate this cumulative sum to its theoretical maximum value (relative cumulative *KBDI*, *rcKBDI*, Eq. A2). Due to its cumulative nature *rcKBDI* is sensitive to changes in both fire season length and fire weather severity.

$$rcKBDI = \frac{\sum_{t=1}^{365} KBDI_t}{800 \cdot 365} \qquad \text{Eq. A2}$$

This composite indicator of drought severity and fire season length is dynamically calculated in the simulation based on the climatic drivers input to the model. In order to modify the empirically specified P_{base} to the climate conditions of the respective simulation year, *rcKBDI* is related to the average index of the reference period for which P_{base} was specified ($rcKBDI_{ref}$, the mean over the period 1501-2000 in this study; Eq. A3).

$$r_{climate} = \frac{rcKBDI}{rcKBDI_{ref}} \qquad \text{Eq. A3}$$

Changes in wildfire suppression activities are accounted for in a similar manner as different fire season conditions. A scalar for fire suppression (r_{mgmt}) is defined relative to the suppression activities of the reference period for which P_{base} was defined. If $r_{mgmt} > 1$ fire suppression is intensified and ignition probability decreased, whereas the opposite is the case if $r_{mgmt} < 1$. For the current study r_{mgmt} was set to 1. The final ignition probability $P_{ignition}$ is calculated via the odds ratio (Wimberly and Kennedy 2008, Eq. A4), and evaluated against a uniform random number to determine whether a fire is ignited in a given cell.

$$odds_{base} = \frac{P_{base}}{1 - P_{base}} \qquad \text{Eq. A4}$$

$$odds_{ignition} = odds_{base} \cdot r_{climate} \cdot r_{mgmt}^{-1}$$

$$P_{ignition} = \frac{odds_{ignition}}{1 + odds_{ignition}}$$

It has to be noted that the thus modeled ignitions do not represent the total number of ignitions on the landscape but relate only to the subset that develops into (detected and recorded) wildfires. In reality there are a (potentially large) number of small ignitions that go undetected and are thus not accounted for in P_{base} (see Malamud et al. 2005).

Fire spread and extinction

Once a fire is ignited at a cell, its spread through the landscape is modeled by means of a cellular automaton approach with 20m horizontal resolution (cf. He and Mladenoff 1999, Wimberly 2002). Transition probabilities are calculated from slope and wind conditions and are further modified by the effects of fuel availability and land type. Slope is calculated from a digital elevation model of 10m horizontal and 1m vertical resolution. Wind speed and direction are supplied as site-specific input to the model, and are randomly modified within a user-specified range for every individual fire in order to mimic the variability of fire conditions in the simulations (Keane et al. 2011). The fire spread to pixels in eight cardinal directions is calculated following FireBGC v2 (Rothermel 1991, Keane et al. 2011), accounting for wind speed and different upslope and downslope spread rates. The thus derived base transition probability (P_{trans}) is further modified for land type and fuel effects. Land types (r_{land}) are specified in a static, spatially explicit input layer and allow, for instance, to account for lower spread rates of fires in riparian areas (cf. Wimberly and Kennedy 2008). The fuel modifier (r_{fuel}) takes into account that a minimum fuel level is necessary for the fire to spread into a cell, and is dynamically calculated in the simulation. Both modifiers are applied to derive the final transition probability (P_{spread}) according to Eq. A5.

$$odds_{trans} = \frac{P_{trans}}{1 - P_{trans}} \qquad \text{Eq. A5}$$

$$odds_{spread} = odds_{trans} \cdot r_{land} \cdot r_{fuel}$$

$$P_{spread} = \frac{odds_{spread}}{1 + odds_{spread}}$$

Every cell only burns for one time step of the cellular automaton, and two pathways of fire extinction are considered in the model. First, a fire extinction probability (P_{ext}) is applied in the simulation of cell-to-cell fire spread, following the approach by Wimberly and Kennedy (2008). If a random number is smaller than P_{ext} the cell is extinguished before it can spread the fire to its neighbors. This parameter is currently a calibration parameter helping to achieve realistic fire patterns on the landscape (see also Wimberly 2002). Its estimation for the current study is described in detail in Appendix B. Second, the overall size of a fire is constrained by a maximum fire size drawn from a fire size distribution (see Wimberly and Kennedy 2008, Sturtevant et al. 2009, Keane et al. 2011). A negative exponential fire size distribution is assumed (He and Mladenoff 1999), and the maximum size of an individual burn (f_{size}) is stochastically determined from the mean fire size of the landscape (f_{mean}) and a uniform random number (*rnd*, Eq. A6).

$$f_{size} = -\log(1 - rnd) \cdot f_{mean} \qquad \text{Eq. A6}$$

The above described cellular automaton approach is run until f_{size} is reached or the simulated fire does not spread to any neighboring pixels in one iteration of the cellular automaton.

Fire severity and effects

Fire severity is modeled following the approach of Schumacher et al. (2006), accounting for the effects of fuel availability, fuel moisture, as well as tree size- and species-specific resistance, while not simulating fire intensity explicitly. As a proxy for fuel availability and fuel structure the iLand detritus pools are used (see Seidl et al. (2012b) for details). The litter pool conceptually corresponds to 1h and 10h fuels (i.e., fast-drying dead foliage and twigs), while the downed woody debris (DWD) pool represents the slower drying 100h and 1000h fuels, i.e., bigger branches and logs. Following Schumacher et al. (2006), the available *fuel* (t biomass per hectare) is calculated from those pools assuming pool-specific moisture relationships (Eq. A7).

$$fuel = \left(kfc_1 + kfc_2 \cdot rcKBDI\right) \cdot FF + kfc_3 \cdot rcKBDI \cdot DWD \qquad \text{Eq. A7}$$

with *FF* the forest floor biomass (t ha^{-1}), and *DWD* the downed woody debris biomass (t ha^{-1}), and kfc_1, kfc_2, and kfc_3 empirical parameters, set to 0.8, 0.2, and, 0.4 (Schumacher et al. 2006). The percentage of crown volume killed depends on fire intensity, tree size and crown form. Fire intensity is related to the amount of fuel available for combustion, and crown kill (*ck*, fraction) is thus modeled as a function of stand size (dbh_{eff}, cm) and available *fuel* (Eq. A8).

$$ck = \min\left(fuel \cdot \left(kck_1 + kck_2 \cdot dbh_{eff}\right);1\right) \qquad \text{Eq. A8}$$

with kck1 and kck2 empirical parameters, determined to be 0.211 and -0.00445 by Schumacher et al. (2006) for Rocky Mountains ecosystems. dbh_{eff} is calculated as average dbh in a 20m cell in iLand, and is limited to <40cm in Eq. A8, assuming a saturation of the crown kill probability for mature stands (see Schumacher et al. 2006). Individual tree mortality probability from fire (P_{mort}) is modeled according to Ryan and Reinhardt (1988) and Keane et al. (2011), using bark thickness and crown kill percentage as predictors (Eq. A9).

$$P_{mort} = \frac{1}{1+e^{-1.941+6.32\cdot\left(1-e^{-bt}\right)-5.35\cdot ck^{2}}} \qquad \text{Eq. A9}$$

where *bt* is bark thickness (cm), calculated from a species-specific empirical parameter from the dbh of a tree (Schumacher et al. 2006, Keane et al. 2011).

Fire effects on forest floor and DWD pools are derived from Eq. A7, i.e., the portion of the respective pools that is considered fuel is also assumed to be consumed by fire. For the trees killed by fire, specific consumption rates are defined for foliage (0.90), branch (0.51), and stemwood (0.11) compartments (see Fahnestock and Agee 1983, Campbell et al. 2007, Mitchell et al. 2009). The remaining C is added to the respective standing and downed detritus pools and treated as the C of trees that die from stress-related or chance mortality in iLand (Seidl et al. 2012b). All trees in the sapling layer (<4m in height) are assumed to be killed by a fire. Soil organic matter is generally not considered to be fuel (Schumacher et al. 2006, Keane et al. 2011), but a small percentage is assumed to be lost within the fire perimeter due to erosion (Campbell et al. 2007, Bormann et al. 2008). More details on the iLand fire module can be found in the online model documentation at http://iLand.boku.ac.at.

References

Andrews, P. L., C. D. Bevins, and R. C. Seli. 2005. BehavePlus fire modeling system version 3.0: User's guide. Page 134. Gen. Tech. Rep. RMRS-GTR-106, Department of Agriculture, Forest Service, Rocky Mountain Research Station, Ogden, UT.

Bormann, B. B. T., P. S. Homann, R. L. Darbyshire, and B. A. Morrissette. 2008. Intense forest wildfire sharply reduces mineral soil C and N: the first direct evidence. Canadian Journal of Forest Research 38:2771–2783.

Campbell, J., D. Donato, D. Azuma, and B. Law. 2007. Pyrogenic carbon emission from a large wildfire in Oregon, United States. Journal of Geophysical Research 112:G04014.

Fahnestock, G. R., and J. K. Agee. 1983. Biomass consumption and smoke production by prehistoric and modern forest fires in western Washington. Journal of Forestry:653–657.

He, H., and D. Mladenoff. 1999. Spatially explicit and stochastic simulation of forest-landscape fire disturbance and succession. Ecology 80:81–99.

Keane, R. E., G. J. Cary, I. D. Davies, M. D. Flannigan, R. H. Gardner, S. Lavorel, J. M. Lenihan, C. Li, and T. S. Rupp. 2004. A classification of landscape fire succession models: spatial simulations of fire and vegetation dynamics. Ecological Modelling 179:3–27.

Keane, R. E., R. A. Loehman, and L. M. Holsinger. 2011. The FireBGCv2 landscape fire succession model : A research simulation platform for exploring fire and vegetation dynamics. Page 137 Simulation. Gen. Tech. Rep. RMRS-GTR-255, Rocky Mountain Research Station, U.S. Department of Agriculture, Forest Service, Fort Collins, CO.

Keetch, J. J., and G. M. Byram. 1968. A drought index for forest fire control. Page 35. U.S. Department of Agriculture, Forest Service, Southeastern Forest Experiment Station, Asheville, NC.

Malamud, B. D., J. D. A. Millington, and G. L. W. Perry. 2005. Characterizing wildfire regimes in the United States. Proceedings of the National Academy of Sciences of the United States of America 102:4694–4699.

Mitchell, S. R., M. E. Harmon, and K. E. B. O'Connell. 2009. Forest fuel reduction alters fire severity and long-term carbon storage in three Pacific Northwest ecosystems. Ecological Applications 19:643–655.

Perry, D. A., P. F. Hessburg, C. N. Skinner, T. A. Spies, S. L. Stephens, A. H. Taylor, J. F. Franklin, B. McComb, and G. Riegel. 2011. The ecology of mixed severity fire regimes in Washington, Oregon, and Northern California. Forest Ecology and Management 262:703–717.

Rothermel, R. C. 1991. Predicting Behavior and Size of Crown Fires in the Northern Rocky Mountains. Page 46 October. Res. Pap. INT-438, U.S. Department of Agriculture, Forest Service, Intermountain Research Station, Ogden, UT.

Ryan, K. C., and E. D. Reinhardt. 1988. Predicting postfire mortality of seven western conifers. Canadian Journal of Forest Research 18:1291–1297.

Schumacher, S., B. Reineking, J. Sibold, and H. Bugmann. 2006. Modeling the impact of climate and vegetation on fire regimes in mountain landscapes. Landscape Ecology 21:539–554.

Seidl, R., P. M. Fernandes, T. F. Fonseca, F. Gillet, A. M. Jönsson, K. Merganičová, S. Netherer, A. Arpaci, J.-D. Bontemps, H. Bugmann, J. R. González-Olabarria, P. Lasch, C. Meredieu, F. Moreira, M.-J. Schelhaas, and F. Mohren. 2011. Modelling natural disturbances in forest ecosystems: a review. Ecological Modelling 222:903–924.

Seidl, R., W. Rammer, R. M. Scheller, and T. A. Spies. 2012a. An individual-based process model to simulate landscape-scale forest ecosystem dynamics. Ecological Modelling 231:87–100.

Seidl, R., T. A. Spies, W. Rammer, E. A. Steel, R. J. Pabst, and K. Olsen. 2012b. Multi-scale drivers of spatial variation in old-growth forest carbon density disentangled with Lidar and an individual-based landscape model. Ecosystems 15:1321–1335.

Sturtevant, B. R., R. M. Scheller, B. R. Miranda, D. Shinneman, and A. Syphard. 2009. Simulating dynamic and mixed-severity fire regimes: A process-based fire extension for LANDIS-II. Ecological Modelling 220:3380–3393.

Wimberly, M. 2002. Spatial simulation of historical landscape patterns in coastal forests of the Pacific Northwest. Canadian Journal of Forest Research 32:1316–1328.

Wimberly, M., and R. Kennedy. 2008. Spatially explicit modeling of mixed-severity fire regimes and landscape dynamics. Forest Ecology and Management 254:511–523.

Appendix B

Parameterization and evaluation of the iLand wildfire module

The parameterization and evaluation of the iLand wildfire module for application at the HJ Andrews Experimental Forest (HJA) focused on the period 1501 to 2000, using the climate, soil, and vegetation data compiled by (Seidl et al. 2012). Topographic information for the HJA watershed was derived from Lidar data (Spies 2011) and was gridded to 10 m horizontal resolution. Key parameters such as mean fire-return interval (at 100 m spatial resolution) and the landscape scale fire size distribution were determined from reconstructions of the fire history at HJA (Teensma 1987, Weisberg 1998, Tepley 2010, Seidl et al. 2012, Tepley et al. 2013).

Model parameterization

To parameterize extinction probability P_{ext}, a crucial parameter for the shape and size of simulated fires in the cellular automaton fire spread routine of iLand (see also Wimberly 2002), a parameterization experiment was designed using fire history data as reference. In this experiment, we started fires with random ignition locations within the reconstructed perimeters of burnt patches. Using the simulated vegetation structure and fuel loads in the year prior to the fire we simulated 100 replicates for each fire recorded in the fire history reconstruction. We independently drew a maximum fire size for every ignition from the historically observed (i.e., reconstructed) distribution (cf. Eq. A6, Appendix A), and randomly drew wind direction (0 to 360°) and wind speed (between 10 and 25 m s^{-1}) for every iteration. From these simulations we iteratively determined P_{ext} by comparing metrics of simulated fire shape to those reconstructed for historical fires. The evaluation metrics used were fractal dimension index, shape index, and the relationship between fire size and fire perimeter (see McGarigal et al. 2002, Wimberly 2002). As starting point for P_{ext} we used data reported by Wimberly (2002). Figures B1 and B2 show the results for an extinction probability of 0.24, which was the endpoint of the parameterization procedure after 23 iterations.

In addition to extinction probability we also adapted the empirical crown kill function implemented in iLand (Eq. A8, Appendix A), originally parameterized for Rocky Mountains ecosystems by Schumacher et al. (2006), to western Cascades ecosystems. The final parameters kck_1 and kck_2 where set to 0.0851 and -0.00185, respectively. With these parameters the mean simulated proportion of low severity fires (47%) compared well to the findings of Weisberg (1998), who estimated it to be 42% for western Cascades landscapes based on tree ring analyses. Furthermore, Agee (1993) reported approximately 16% high severity patches in mountain forests of the southern Oregon Cascades, which is close to the simulated 20% (mean over all simulated fires in the parameterization experiment). Generally, the model simulated a mixed severity fire regime for the HJA (Figure B3), which is in line with the analysis of Perry et al. (2011), who report a mixed severity regime (with a considerable share of high severity patches) for Douglas-fir/ western hemlock forest types.

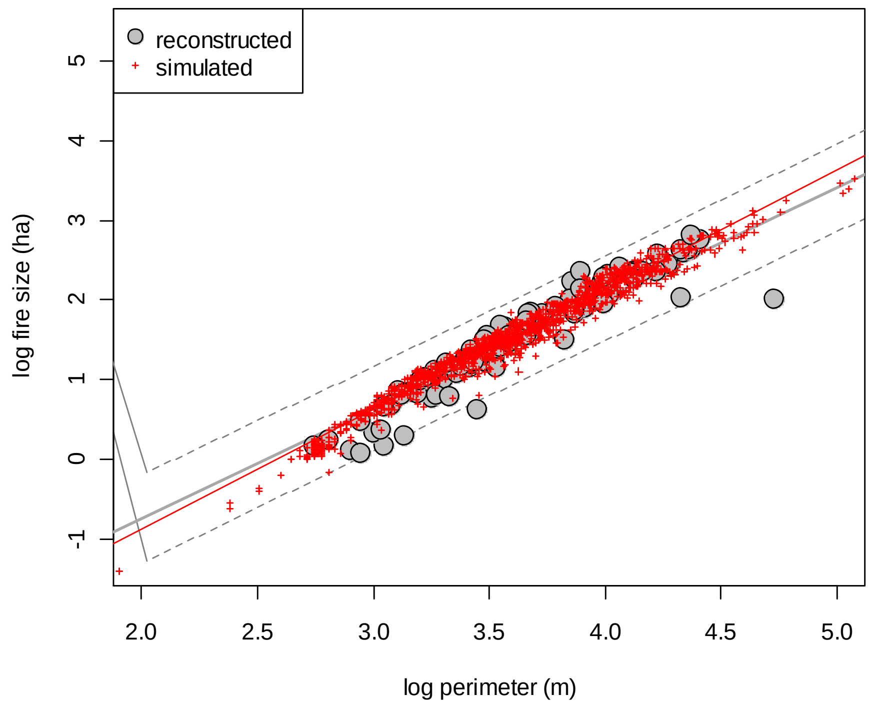

Figure B1: Fire size over fire perimeter for reconstructed fire patches (grey) and simulated fire patches (red). Solid lines give linear relationships in log-log space, with dashed grey lines the confidence interval of the linear model for reconstructed fires.

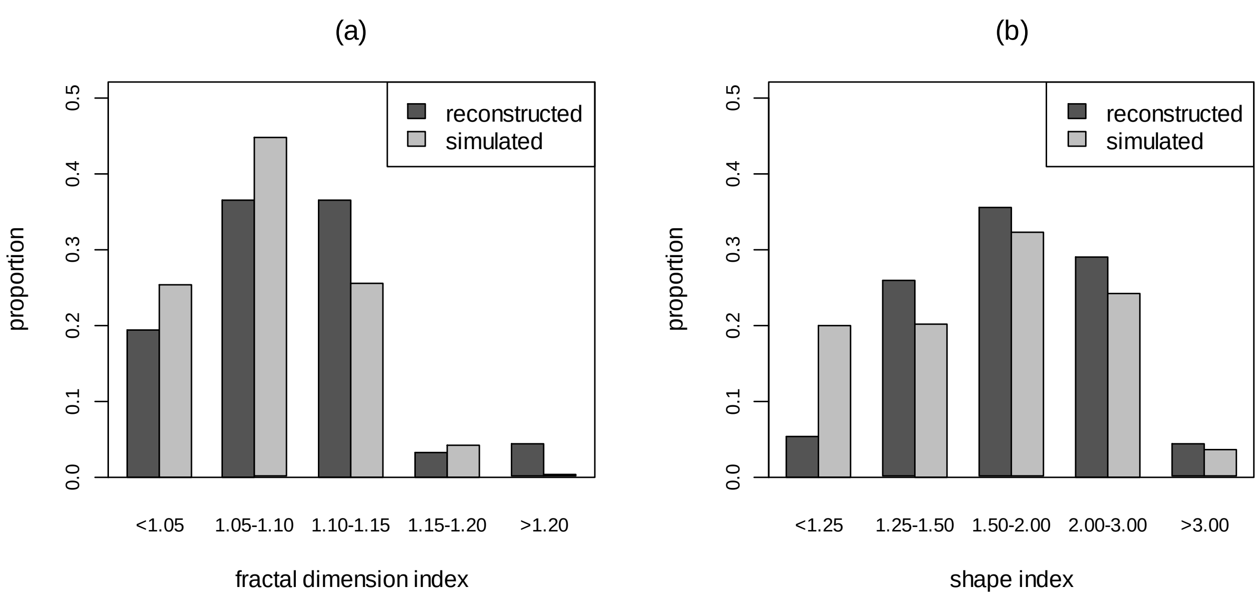

Figure B2: Reconstructed and simulated fire shapes for fire patches at the HJA after parameterization. For description of the fire complexity metrics fractal dimension index and shape index see McGarigal et al. (2002).

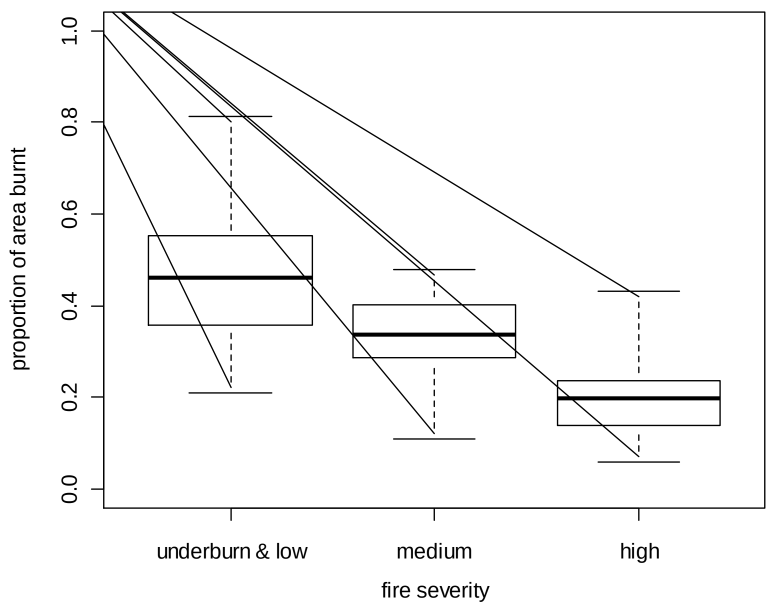

Figure B3: Simulated fire severity at the HJ Andrews Experimental Forest. Boxplots indicate the distribution of proportion of area burnt over severity classes for 100 replicated fires in each of the 13 fire years reconstructed for the period 1501 to 2000. The central indicator gives the median value, boxes indicate the interquartile range, and whiskers extend to the extreme values.

Model evaluation

After parameterizing the model we conducted a series of simulation runs from 1501 to 2000 to evaluate the full dynamic behavior of the model (i.e., the interactions between stand dynamics, fuel buildup, fire occurrence, spread, severity, and feedbacks on vegetation development), and assess whether a realistic fire regime is emerging from dynamic iLand simulations at HJA. These runs were started from the last landscape-level burn in year 1500 (legacy scenario L1), and ten replicated 500 year simulations were conducted. To evaluate the model we compared the simulated fire size distribution as well as the mean fire return interval to expectations from fire history reconstructions for the HJA landscape. The simulated mean fire size over all fires and replicates (916 ha) corresponded well to the reconstructed mean fire size for the HJA (965 ha). Furthermore, the strongly skewed fire size distribution resulting from the simulations is well in line with expectations (Figure B4). The dynamically simulated mean fire return interval (MFRI) of 218 years for the entire HJA landscape was slightly lower than the reconstructed value (262 years). However, the expected pattern of decreasing MFRI with increasing elevation was reproduced by the dynamic fire simulations with iLand (Figure B5).

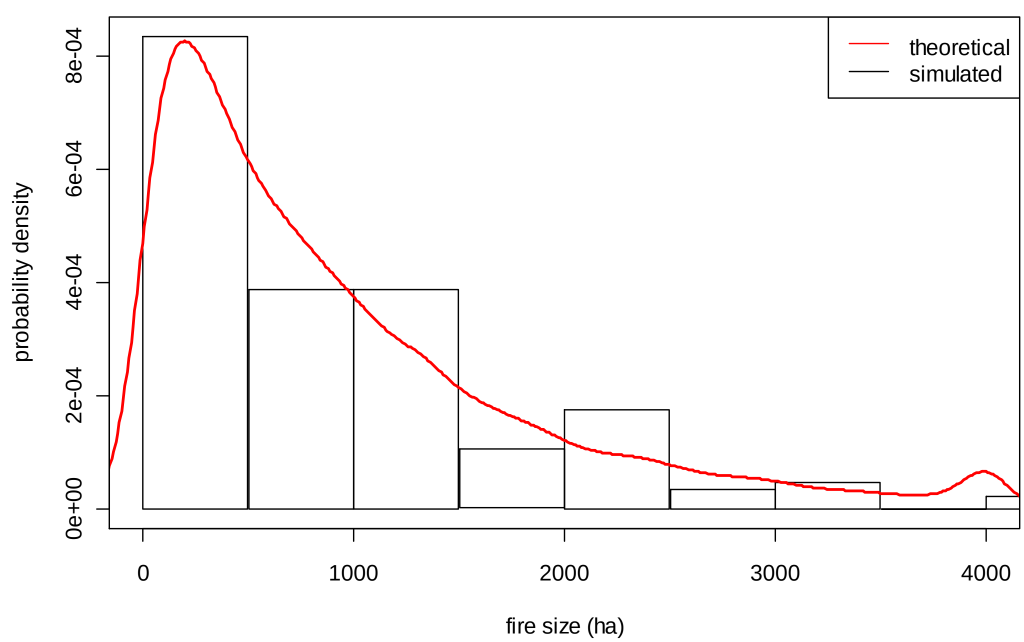

Figure B4: Simulated versus theoretically expected fire size distribution (assuming a min-max constrained negative exponential fire size distribution, parameterized with reconstructed mean fire size). Simulation results are derived from ten replicated 500 year simulations.

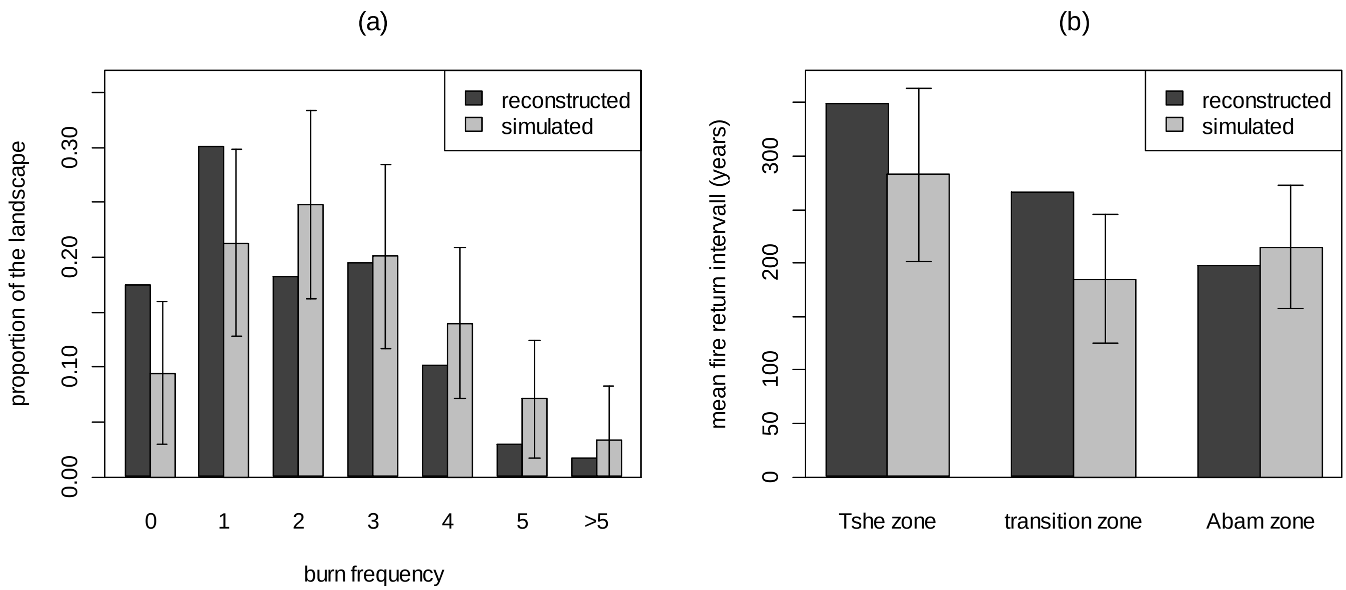

Figure B5: (a) Reconstructed and simulated burn frequency in the years 1501 - 2000 at HJA. (b) Reconstructed and simulated mean fire return interval in the three major vegetation zones at HJA. Tshe: Tsuga heterophylla zone (low elevation), transition zone (mid elevation), Abam: Abies amabilis zone (high elevation). Whiskers indicate the standard deviation around the mean of 10 replicated simulation runs.

References

Agee, J. K. 1993. Fire ecology of Pacific Northwest forests. Page 505. Island Press, Washington, DC.

McGarigal, K., S. Cushman, M. Neel, and E. Ene. 2002. FRAGSTATS: Spatial Pattern Analysis Program for Categorical Maps. Computer software program produced by the authors at the University of Massachusetts, Amherst. http://www.umass.edu/landeco/research/fragstats/fragstats.html.

Perry, D. A., P. F. Hessburg, C. N. Skinner, T. A. Spies, S. L. Stephens, A. H. Taylor, J. F. Franklin, B. McComb, and G. Riegel. 2011. The ecology of mixed severity fire regimes in Washington, Oregon, and Northern California. Forest Ecology and Management 262:703–717.

Schumacher, S., B. Reineking, J. Sibold, and H. Bugmann. 2006. Modeling the impact of climate and vegetation on fire regimes in mountain landscapes. Landscape Ecology 21:539–554.

Seidl, R., T. A. Spies, W. Rammer, E. A. Steel, R. J. Pabst, and K. Olsen. 2012. Multi-scale drivers of spatial variation in old-growth forest carbon density disentangled with Lidar and an individual-based landscape model. Ecosystems 15:1321–1335.

Spies, T. A. 2011. LiDAR data (August 2008) for the Andrews Experimental Forest and Willamette National Forest study areas. H. J. Andrews Experimental Forest. Forest Science Data Bank, Corvallis, OR. http://andrewsforest.oregonstate.edu/data/abstract.cfm?dbcode=GI010.

Teensma, P. D. A. 1987. Fire history and fire regimes of the central western Cascades of Oregon. University of Oregon.

Tepley, A. J. 2010. Age structure, developmental pathways, and fire regime characterization of Douglas-fir/ western hemlock forests in the Central Western Cascades of Oregon. Oregon State University.

Tepley, A. J., F. J. Swanson, and T. A. Spies. 2013. Fire-mediated pathways of stand development in Douglas-fir/ western hemlock forests of the Pacific Northwest, USA. Ecology:in press.

Weisberg, P. J. 1998. Fire history, fire regimes, and development of forest structure in the Central Western Oregon Cascades. Oregon State University.

Wimberly, M. 2002. Spatial simulation of historical landscape patterns in coastal forests of the Pacific Northwest. Canadian Journal of Forest Research 32:1316–1328.

Appendix C

Additional results and analyses of legacy effects on forest ecosystem structure, composition, and functioning

Appendix C gives additional simulation results and presents additional analyses with the aim to aid the interpretation of the results and conclusions presented in the main paper. Table C1 gives the scenario differences in TEC, RI, and LSS for four points in time, and tests their significance relative to the scenario assuming historic legacy levels and disturbance regimes (L1F1). Table C2 presents annualized change rates in the same ecosystem indicators for different time periods. Figure C1 shows the progression of live C density over time at the landscape scale in different legacy scenarios, and indicates that initial live tree legacies persist well into the second century of the 500-year study period (cf. Figure 3). As a test of differences in the multi-indicator phase space of TEC, RI, and LSS Table C3 contains a distance measure between the scenarios as well as a test for its statistical significance, given the within- and between scenario variation. Finally, Table C4 presents further results from the simulation model with regard to important indicators of ecosystem functioning, aiding the causal interpretation of our findings.

Table C1: Scenario differences in four points in time, relative to the simulations assuming historic legacy levels and disturbance regime (L1F1). Differences were tested for significance by means of a Wilcoxon signed rank sum test, and significant values (α=0.05) are highlighted in bold.

legacy	fire frequency	functioning TEC (Mg C ha^{-1})				structure RI (dimensionless)				composition LSS (%)			
		year 1	year 51	year 151	year 501	year 1	year 51	year 151	year 501	year 1	year 51	year 151	year 501
L0	F0	-30.9	**-117.4** (<0.001)	**-31.6** (<0.001)	**+133.7** (<0.001)	-0.14	**-0.28** (<0.001)	**-0.59** (<0.001)	**-0.61** (<0.001)	-17.1	**-24.8** (<0.001)	**-22.0** (<0.001)	**-3.3** (<0.001)
	F1	-30.9	**-125.5** (<0.001)	**-76.9** (<0.001)	+37.2 (0.054)	-0.14	**-0.25** (<0.001)	**-0.36** (<0.001)	-0.07 (0.271)	-17.1	**-24.3** (<0.001)	**-29.9** (<0.001)	**-15.2** (<0.001)
	F2	-30.9	**-131.3** (<0.001)	**-105.1** (<0.001)	**-40.4** (0.035)	-0.14	**-0.23** (<0.001)	**-0.21** (<0.001)	**+0.29** (<0.001)	-17.1	**-24.8** (<0.001)	**-33.5** (<0.001)	**-30.0** (<0.001)
L1	F0	±0.0	**+20.3** (<0.001)	**+56.3** (<0.001)	**+125.7** (<0.001)	±0.00	**-0.08** (<0.001)	**-0.33** (<0.001)	**-0.65** (<0.001)	±0.0	**+2.0** (0.004)	**+10.7** (<0.001)	**+9.1** (<0.001)
	F1	–	–	–	–	–	–	–	–	–	–	–	–
	F2	±0.0	-8.8 (0.152)	**-50.5** (<0.001)	**-78.4** (<0.001)	±0.00	**+0.03** (0.263)	**+0.23** (<0.001)	**+0.23** (0.001)	±0.0	-1.6 (0.207)	**-8.3** (<0.001)	**-16.9** (<0.001)
L2	F0	+29.9	**+64.8** (<0.001)	**+67.2** (<0.001)	**+113.1** (<0.001)	+0.09	**+0.05** (<0.001)	**-0.12** (0.004)	**-0.62** (<0.001)	+13.5	**+11.3** (<0.001)	**+14.7** (<0.001)	**+9.1** (<0.001)
	F1	+29.9	**+42.1** (<0.001)	**+25.8** (0.012)	+11.3 (0.603)	+0.09	**+0.14** (<0.001)	**+0.10** (0.039)	**-0.14** (0.018)	+13.5	**+9.0** (<0.001)	**+8.7** (<0.001)	+2.1 (0.255)
	F2	+29.9	**+31.0**	**-41.5**	**-93.0**	+0.09	**+0.19**	**+0.39**	**+0.18**	+13.5	**+7.7**	-1.0	**-17.3**

	(<0.001)	(0.002)	(<0.001)		(<0.001)	(<0.001)	(0.005)		(<0.001)	(0.631)	(<0.001)

Table C2: Annualized change rates in ecosystem indicators in three different periods of time. Values in parenthesis indicate the 5th-95th percentile range over the 25 replicated simulations.

legacy	fire frequency	functioning TEC ($Mg\ C\ ha^{-1}\ yr^{-1}$)			structure RI (dimensionless $10^{-2}\ yr^{-1}$)			composition LSS (% yr^{-1})		
		yrs 1-50	yrs 1-100	yrs 401-500	yrs 1-50	yrs 1-100	yrs 401-500	yrs 1-50	yrs 1-100	yrs 401-500
L0	F0	-6.40	-2.24	+0.58	+0.089	+0.092	+0.559	+0.189	+0.239	+0.111
	F1	-6.56 (-6.89 - -6.39)	-2.47 (-2.92 - -2.26)	+0.37 (-0.43 - +1.06)	+0.141 (+0.087 - +0.278)	+0.189 (+0.094 - +0.385)	+0.467 (+0.105 - +0.972)	+0.197 (+0.127 - +0.255)	+0.198 (+0.132 - +0.235)	+0.118 (+0.013 - +0.180)
	F2	-6.68 (-7.00 - -6.41)	-2.68 (-3.00 - -2.37)	+0.23 (-1.04 - +1.08)	+0.168 (+0.085 - +0.354)	+0.281 (+0.150 - +0.408)	+0.400 (+0.068 - +0.759)	+0.187 (+0.100 - +0.239)	+0.171 (+0.113 - +0.224)	+0.104 (-0.031 - +0.216)
L1	F0	-4.27	-1.07	+0.49	+0.200	+0.171	+0.343	+0.381	+0.388	+0.022
	F1	-4.67 (-5.61 - -4.29)	-1.48 (-2.04 - -1.11)	+0.00 (-1.40 - +1.17)	+0.367 (+0.207 - +0.748)	+0.380 (+0.188 - +0.660)	+0.411 (+0.109 - +0.788)	+0.341 (+0.264 - +0.399)	+0.317 (+0.237 - +0.399)	+0.069 (-0.039 - +0.205)
	F2	-4.83 (-5.95 - -4.35)	-1.70 (-2.31 – 1.22)	+0.13 (-1.19 - +1.28)	+0.430 (+0.228 - +1.121)	+0.478 (+0.241 - +0.786)	+0.258 (-0.263 - +0.867)	+0.309 (+0.101 - +0.394)	+0.279 (+0.175 - +0.382)	+0.067 (-0.044 - +0.183)
L2	F0	-3.97	-1.13	+0.45	+0.294	+0.253	+0.268	+0.297	+0.306	+0.015
	F1	-4.41 (-4.99 - -3.98)	-1.37 (-1.84 - -1.13)	+0.34 (-0.41 - +1.35)	+0.478 (+0.291 - +0.852)	+0.392 (+0.277 - +0.597)	+0.271 (+0.011 - +0.555)	+0.252 (+0.159 - +0.312)	+0.275 (+0.205 - +0.324)	+0.060 (-0.042 - +0.193)
	F2	-4.64	-1.98	-0.05	+0.579	+0.670	+0.314	0.223	+0.196	+0.024

	(-5.28 - -4.12)	(-2.85 - -1.59)	(-1.36 - +0.89)	(+0.313 - +0.955)	(+0.383 - +1.119)	(+0.050 - +0.702)	(+0.126 - +0.301)	(+0.076 - +0.266)	(-0.112 - +0.142)

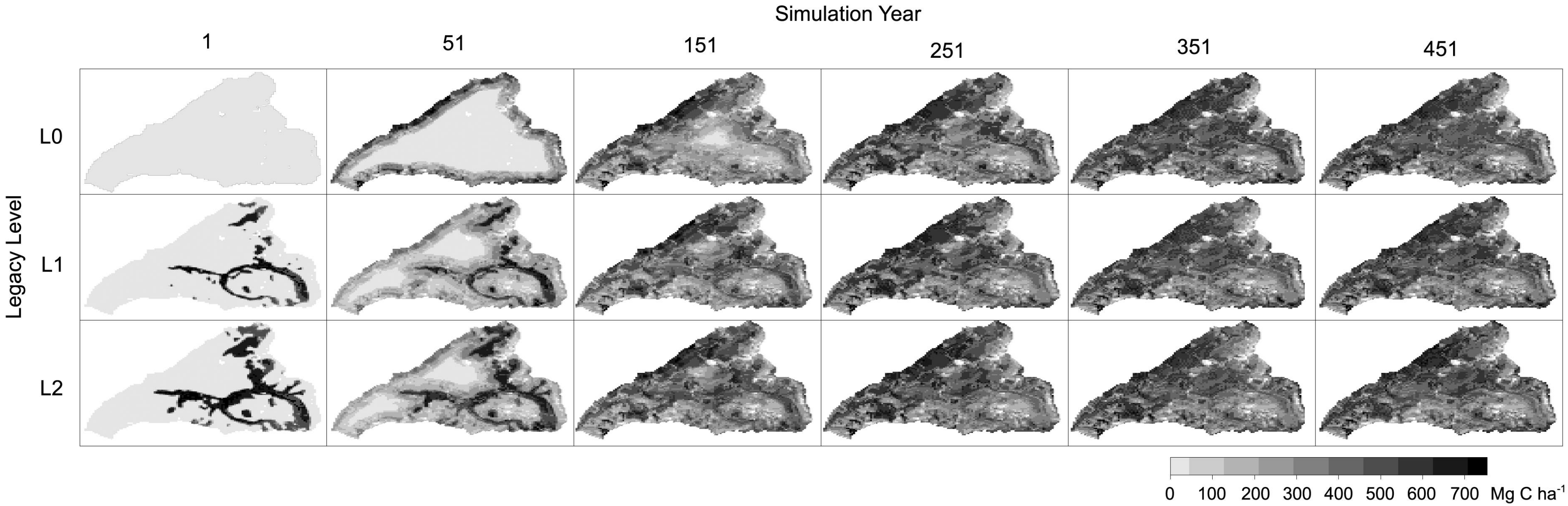

Figure C1: Maps of the 6364-ha HJ Andrews Experimental Forest landscape (grain: 100m grid), showing live ecosystem carbon for six points in time and three legacy levels (L0: no legacies, L1: 12% legacies, L2: 24% legacies). The values are cell-level means over 25 replicated simulations per series and assume the historically observed mean fire return interval of 262 years (scenario F1).

Table C3: Distance between the ecosystem states in the phase space of TEC, RI, and LSS at the end of the 500-year simulation period, expressed by the squared Mahalanobis distance (D^2). D^2 is a multidimensional version of a z-score, measuring the distance of a case from the centroid (multidimensional mean) of a distribution, given the covariance (multidimensional variance) of the distribution. Significance levels refer to a X^2 test (with three degrees of freedom), and significant values (α=0.05) are highlighted in bold.

		L0			L1			L2		
		F0	F1	F2	F0	F1	F2	F0	F1	F2
L0	F0	-								
	F1	**10.2 (0.017)**	-							
	F2	**55.5 (<0.001)**	4.0 (0.257)	-						
L1	F0	**172.4 (<0.001)**	**26.7 (<0.001)**	**83.6 (<0.001)**	-					
	F1	**21.4 (<0.001)**	**14.5 (0.002)**	**32.8 (<0.001)**	**18.8 (<0.001)**	-				
	F2	**33.3 (<0.001)**	**8.9 (0.031)**	**13.3 (0.004)**	**33.2 (<0.001)**	4.1 (0.247)	-			
L2	F0	**157.0 (<0.001)**	**29.3 (<0.001)**	**88.9 (<0.001)**	4.1 (0.247)	**19.0 (<0.001)**	**31.6 (<0.001)**	-		
	F1	**49.2 (<0.001)**	**23.3 (<0.001)**	**46.0 (<0.001)**	**26.6 (<0.001)**	1.2 (0.765)	7.6 (0.054)	**22.8 (<0.001)**	-	
	F2	**41.5 (<0.001)**	**9.1 (0.028)**	**10.7 (0.014)**	**35.2 (<0.001)**	3.7 (0.292)	0.5 (0.908)	**31.9 (<0.001)**	4.6 (0.201)	-

Table C4: Simulation results for leaf area index (LAI), net primary productivity (NPP), and carbon in the litter and soil compartments over the three legacy (L) and fire frequency (F) scenarios. Values in parenthesis indicate the 5th-95th percentile range over the 25 replicated simulations.

legacy	fire frequency	LAI (m^2 m^{-2})			NPP (Mg C ha^{-1} yr^{-1})			litter and soil C (Mg C ha^{-1})		
		yrs 1-100	yrs 401-500	yrs 1-500	yrs 1-100	yrs 401-500	yrs 1-500	yrs 1-100	yrs 401-500	yrs 1-500
L0	F0	3.56	6.22	5.78	6.07	7.84	8.02	104.5	142.6	130.0
	F1	3.27 (2.82 – 3.55)	5.77 (4.84 – 6.59)	5.30 (4.74 – 5.70)	5.78 (5.41 – 6.06)	7.53 (7.00 – 7.93)	7.64 (7.28 – 7.92)	102.1 (98.2 – 104.3)	131.8 (117.7 – 144.4)	120.3 (109.4 – 127.2)
	F2	3.02 (2.59 – 3.34)	4.66 (4.09 – 5.40)	4.50 (4.12 – 4.91)	5.55 (5.13 – 5.90)	6.84 (6.21 – 7.45)	7.08 (6.76 – 7.40)	100.2 (96.3 – 102.9)	111.3 (99.0 – 123.4)	106.6 (99.1 – 115.7)
L1	F0	4.72	6.58	6.14	7.28	8.09	8.26	126.0	150.6	141.4
	F1	4.31 (3.78 – 4.68)	5.43 (4.58 – 6.27)	5.31 (4.93 – 5.81)	6.91 (6.47 – 7.21)	7.39 (6.66 – 7.94)	7.71 (7.40 – 8.02)	121.8 (116.2 – 125.4)	129.5 (116.3 – 142.7)	126.4 (118.2 – 135.1)
	F2	4.04 (3.42 – 4.55)	4.54 (3.93 – 5.47)	4.62 (4.31 – 5.02)	6.68 (6.06 – 7.14)	6.81 (6.17 – 7.70)	7.18 (6.95 – 7.49)	119.3 (111.9 – 124.7)	109.1 (95.5 – 123.6)	112.7 (107.4 – 120.7)
L2	F0	4.97	6.61	6.17	7.39	8.08	8.22	131.2	152.1	143.3
	F1	4.61 (4.07 – 4.92)	5.54 (4.74 – 6.24)	5.45 (5.14 – 5.80)	7.07 (6.55 – 7.36)	7.59 (7.07 – 8.07)	7.78 (7.59 – 8.00)	126.9 (121.6 – 130.7)	130.8 (120.4 – 142.5)	129.8 (123.5 – 136.9)
	F2	4.19 (3.61 – 4.52)	4.58 (3.80 – 5.53)	4.64 (4.23 – 5.07)	6.71 (6.04 – 7.08)	6.76 (6.08 – 7.66)	7.15 (6.76 – 7.52)	123.6 (117.0 – 127.6)	110.9 (92.0 – 128.4)	114.2 (106.7 – 122.4)